Multi-scale Simulations of Partially Unzipped CNT Hetero-junction Tunneling Field Effect Transistor

Larkhoon Leem[1], Ashutosh Srivastava[2], Shuang Li[3], Blanka Magyari-Köpe[1], Giuseppe Iannaccone[4], James S. Harris[1], Gianluca Fiori[4]

[1]Department of Electrical Engineering, [2]Department of Materials Science and Engineering, [3]Department of Physics, Stanford University, 420 Via Palou, 94305, Stanford, U.S.A.
[4]Dipartimento di Ingegneria dell'Informazione, Universita di Pisa, via Caruso, 56122, Pisa, Italy

Abstract

Band-to-band Tunneling Field Effect Transistors (TFETs) are emerging as a solution to break classical 60mV/dec sub-threshold slope limit of conventional MOSFETs. In this work, we present for the first time multi-scale simulation results of partially unzipped Carbon Nanotube heterojunction TFET. Compared to the CNT and GNR homojunction TFETs, GNR/CNT heterojunction TFETs demonstrate superior sub-threshold region characteristics – 10^4× smaller I_{off}, 61% smaller Subthreshold Swing (SS) which lies in the range of 22~26mV/dec and the I-V ambipolarity is completely eliminated.

Introduction

With all the fruits harvested from the low-power CMOS design tree, it has become clear that further improvements in energy efficiency will only be realized through novel and revolutionary changes in MOSFET design [1]. Band-to-band Tunneling Field Effect Transistors (TFETs) have recently attracted deep interest in the research community because of their small sub-threshold slope (SS). Conventional MOSFETs operate by thermal injection over channel barrier limiting the SS to 60mV/decade. In contrast, TFETs exploit interband quantum mechanical tunneling as the device operation mechanism, leading to small SS and reduced power supply voltage for digital logic applications. While a number of band-to-band tunneling transistors have been reported to achieve SS < 60mV/dec [2], their potential applications are limited by: 1) small I_{on} current as compared to conventional MOSFETs, 2) ambipolar I-V characteristics, and 3) SS < 60mV obtained only in a very limited V_{gs} interval. In this work, we present for the first time, multi-scale approach consisting of Density-Functional Theory (DFT), Extended Hückel Theory (EHT), Molecular Dynamics (MD) and atomistic Tight-Binding (TB) calculations to simulate Carbon nanostructure-based TFETs with type-II tunneling barriers that results from partially unzipping Carbon Nanotubes (CNTs). The concept of unzipping CNT [3,4,5] (Fig. 1,2) is promising because one can obtain high quality GNRs with reduced roughness [3]. In addition, partially unzipped CNT has been shown to significantly diminish the tunneling barrier [6]. In this work, we numerically demonstrate for the first time that partially unzipping CNT can induce type-II heterojunction between GNR and primitive CNT to overcome the limitations of TFETs mentioned above.

Device operating principle

The I-V curve ambipolarity of homojunction TFETs results from the symmetric energybands at device ON and OFF states: the energy bandgap at the source and channel junction becomes narrower when V_{gs} >0. The energy bandgap at the drain and channel junction symmetrically

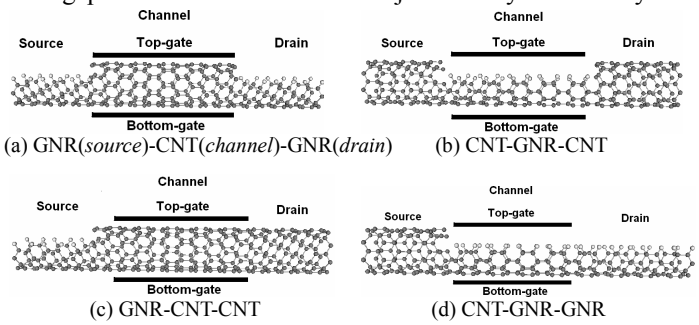

Figure 1. Partially unzipped Carbon Nanotube (CNT) Heterojunction Tunneling FET (TFET) Cross-sectional schematics of simulated Graphene Nanoribbon (GNR)/CNT heterojunctions to study their effects on the Tunneling FET performance (a)~(d).

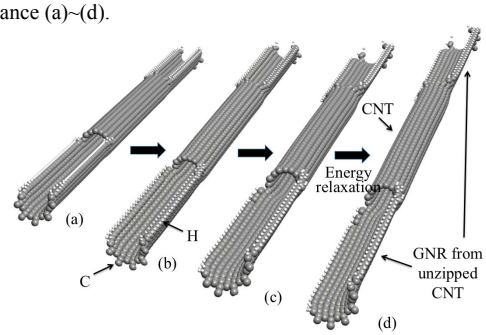

Figure 2. Energy-relaxed configurations of partially unzipped CNT obtained from Molecular Dynamics (MD) simulations. Initial (a) and final energy stabilized configuration (d).

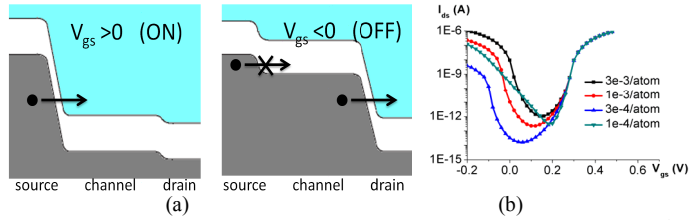

Figure 3. Symmetric energy bands of Homojunction TFETs. Energyband diagrams of a homojunction TFET when V_{gs} >0 and V_{gs} < 0, respectively (a). Tunneling happens for both V_{gs} >0 and V_{gs} <0, which leads to I-V ambipolarity in (b) of homojunction CNT TFET. Ambipolarity prevails even the doping levels (in molar fractions) in drain region were optimized as in [7].

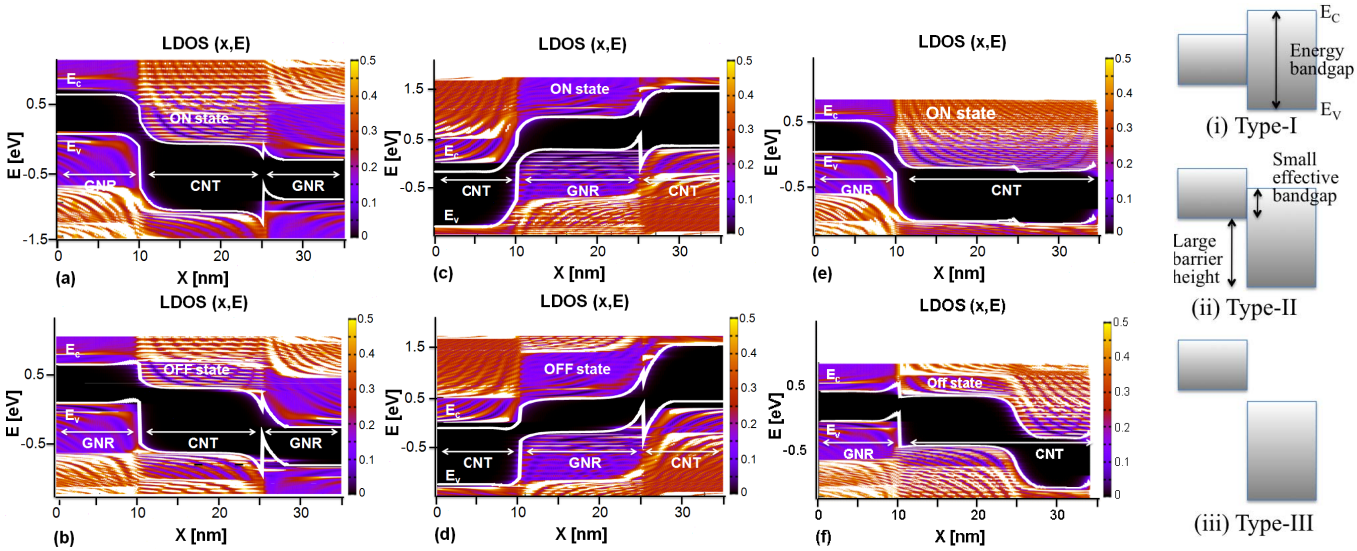

Figure 4. Band diagram (white solid lines) and local density of states (LDOSs) of GNR/CNT tunneling FETs. GNR-CNT-GNR (left column), CNT-GNR-CNT (center) and GNR-CNT-CNT (right) configurations are shown for ON (top row) and OFF state (bottom row). CNT(8,0) is partially unzipped to create GNR n=16 at source/drain or channel regions. Due to the workfunction and bandgap differences between the GNR and CNT, type-II (staggered) heterojunctions are formed. Notably, the symmetric energyband diagrams as in Fig. 3(a) are not found in our GNR/CNT heterojunction TFETs.

gets narrow to incur large OFF current when V_{gs} <0 (Fig. 3(a)). A well-defined approach based on physics to suppress this ambipolarity is to break the symmetry with asymmetric doping (Fig. 3(b)) or gate electrode location [7]. However, these techniques do not eliminate I-V ambipolarity and the effectiveness is limited to narrow V_{gs} range (Fig. 3(b)) [7]. Interestingly, heterojunctions can fundamentally break this symmetry, leading to excellent sub-threshold region characteristics: large bandgap material is used for the channel and drain region to suppress the tunneling at the drain-channel junction while, small bandgap material is selected for the source region to increase the tunneling I_{on}. Among various heterojunction types (Fig. 4 i~iii), type-II is preferred over type-I because of smaller bandgap overlap or *effective bandgap* to facilitate I_{on} tunneling and higher energy barrier to impede I_{off} current flow [8]. This type-II heterojunction in carbon nanostructure can be easily achieved by partially unzipping the CNTs. When CNTs are partially unzipped, there exist a difference in energy bandgaps and workfunctions between the primitive and unzipped CNT, which can lead to type-II heterojunctions.

Device simulation process

The flow diagram of our multi-scale approach is shown in Fig. 5. Electronic structure such as energy bandgap and workfunctions of GNR and CNTs were calculated using DFT, EHT [9]. Carbon-based heterostructure was energy-relaxed through DFT simulation at T=0K. Then, the 3D-Poisson equation within the Non-Equilibrium Green's function Formalism (NEGF) and Tight-Binding methods were used to calculate I-V characteristics of the device. DFT/EHT calculation was done using Atomistix ToolKit version 2008.10.0, 2010.02 and 10.08.0 [10], I-V characteristics calculation fully exploited the open-source NanoTCAD ViDES simulator [11] and MD simulation used LAMMPS simulator [12]. For bandgap, workfunction and I-V calculations, GNR with no curvature and abrupt junction between GNR and CNT were assumed. This was to reduce the number of atoms in DFT calculations but also, our I-V calculations indicated that TFETs with "completely rolled GNR" and "flat GNR" as the channel region had the I_{ds} difference of 4.6% or less (Fig. 6). More realistic curvature information on unzipped CNTs was obtained from MD simulation (Fig. 2) that includes long range Coulombic interaction among atoms (2507 C, H atoms). This result will be included in the rest of the simulation process in a future work. Four different device configurations (Fig. 1(a)~(d)) have been investigated for optimal device performance according to

CNT (N,0)	GNR (n)	E_{g_CNT} (DFT)	E_{g_CNT} (EHT)	ϕ(CNT)	ϕ(CNT) [Ref. 14]	E_{g_GNR} (DFT)	E_{g_GNR} (EHT)	ϕ(GNR)	ϕ(GNR) [Ref. 15]	ϕ(GNR) - ϕ(CNT)	Type -II	Type -III	E_{g_eff},* effective bandgap
14	24	0.612eV	0.64 eV	3.783 eV	~4.7eV	0.295eV	0.352 eV	3.628 eV	~4.58 eV	-0.0111 eV	√		0.3409 eV
13	22	0.7364	0.77	3.8215		0.491	0.46	3.618		-0.0485	√		0.4115
11	16	0.766	0.79	3.745		0.672	0.624	3.582		-0.08	√		0.544
10	16	0.937	1.01	3.813						-0.038	√		0.586
8	16	0.57	1.054	4.017	4.8					-0.22	√		0.404
7	14	0.497	1.184	4.201	5.1	0.12	0.047	3.567		-0.0655		√	-0.0185

Table 1. Calculated electronic structures of partially unzipped CNT using first principles methods. E_g: energy bandgap, ϕ: workfunction, the energy difference between the vacuum level and the Fermi level. For I-V calculations, we used the energy bandgaps of CNT and GNR obtained from Extended Hückel Theory (EHT) and the rest from Density Functional Theory (DFT). *E_{g_eff} is an overlap between two bandgaps (Fig. 4 (ii)).

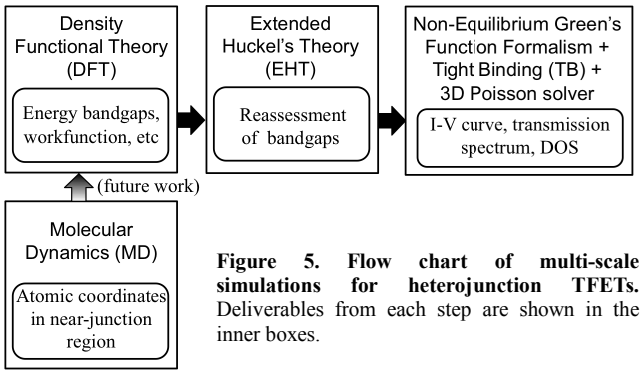

Figure 5. Flow chart of multi-scale simulations for heterojunction TFETs. Deliverables from each step are shown in the inner boxes.

ITRS requirements [13]. The nominal device has double-gate geometry with 1.7 nm thick SiO_2 gate oxide. The channel length, L_{ch}=15nm, the source/drain extension, $L_{S|D}$ is 10nm. The source/drain used <=3e-3/atom doping levels in molar fractions.

Device simulation results

Table 1 shows the energy bandgaps and workfunctions of CNTs and unzipped CNTs calculated from DFT and EHT methods in this work. Considering the possible loss of Carbon atoms during unzipping (e.g., by controlling etching time), a number of different types of GNRs can be produced from a single chirality of CNT. Calculated results indicate that the workfunction of CNT is a function of nanotube diameter. On the other hand, unzipped CNTs are found to have almost constant workfunctions because zero curvature GNRs are assumed. Example combinations of zig-zag CNTs and armchair GNRs that make type-II heterojunctions are listed in Table 1. Among these combinations, CNT (8,0) and a-GNR n=16 are chosen for further I-V calculations because of its small bandgap overlap between CNT and GNR while E_g of CNT is large. The DFT calculations were done using the geometrical relaxation to a force tolerance limit of 0.05eV/Angstrom. Difference in this limit could have led to slight variations in the workfunction values compared to other related works [14,15].

Fig. 2 illustrates the energy relaxation process of partial unzipping of CNT (8,0) through MD simulations. Completely stabilized configuration showed 3~4nm of curved GNR region before GNRs becoming completely flat.

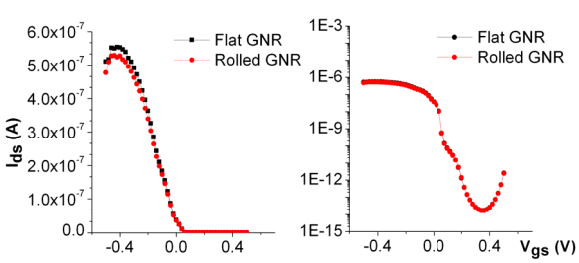

Figure 6. I-V characterisitics of heterojunction TFETs with unrolled GNR ("flat") vs. completely rolled GNR. I-V curves of the CNT-GNR-CNT with unrolled and rolled GNRs are compared (left plot in linear scale and the right plot in log scale). For the worst case estimation, CNT(source)-GNR(channel)-CNT(drain) configuration is used, whose device turns on at V_{gs} <0 as shown in the plot.

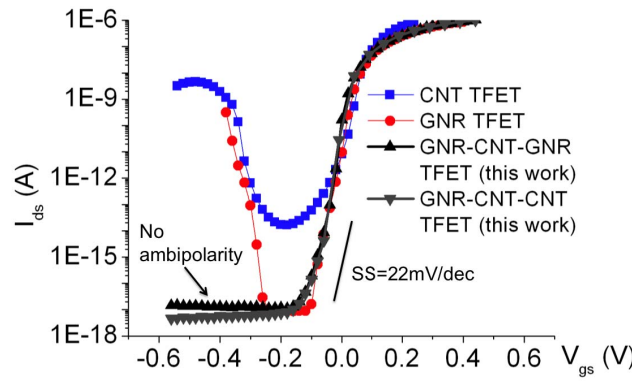

Figure 7. Comparison of I-V curves of Carbon based tunneling FETs. The workfunction of the gate electrode is adjusted to have $I_{ds}=10^{-11}$A is at V_{gs}=0V. Compared to CNT TFET, GNR/CNT heterojunction TFET shows smaller I_{off} ,SS and I-V ambipolarity completely suppressed while they show comparable performance with GNR TFET.

In Fig. 4, the Density-of-State (DOS) plots of the GNR/CNT heterojunction TFETs are shown for ON (top row) and OFF state (bottom row). CNT (8,0) is partially unzipped to create a-GNR n=16 at source/drain or channel regions. Due to the heterojunctions, symmetric energy bands present in homojunction TFETs are removed. For example, in GNR(*source*)-CNT(*channel*)-CNT(*drain*) TFET, tunneling is enhanced in the ON state due to smaller effective bandgap (Fig. 4(e)). In the OFF state, tunneling is strongly suppressed by larger bandgap channel material and high energy barrier of type-II heterojunction (Fig. 4(f)).

Compared to the CNT and GNR homojunction TFETs, GNR/CNT heterojunction TFETs demonstrate superior sub-threshold region characteristics - $10^4\times$ smaller I_{off}, 61% smaller SS=22~26mV/dec (compared with CNT-TFET) and I-V ambipolarity is completely suppressed (Fig. 7). This is because of 1) the availability of larger bandgap material for the channel (CNT (8,0) in the GNR/CNT heterojunction, E_g=1.054eV) 2) the smaller bandgap material (a-GNR n=16, E_g=0.624eV) for the source region and 3) type-II heterojunction for the source and channel interface (effective E_g=0.44eV). For fair comparisons with GNR/CNT heterojunction TFETs, CNT and GNR homojunction TFETs were optimized for the best performance. Doping levels (in molar fractions) in the drain region were reduced (as compared to the source region) to suppress the ambipolarity. In addition, CNT (14,0) (E_g=0.64eV) was chosen for CNT TFET to match the E_g=0.624eV of GNR n=16.

Among four heterojunction configurations (Fig. 1(a)~(d)), GNR-CNT-GNR and GNR-CNT-CNT demonstrate better substhreshold slope and I_{off} than the rest. This is due to large energy bandgap material in the channel and drain region (GNR-CNT-CNT) and high energy barrier at the channel-drain junction (GNR-CNT-GNR). There were no significant differences in I-V characteristics between the two configurations (Fig. 7), indicating that it is

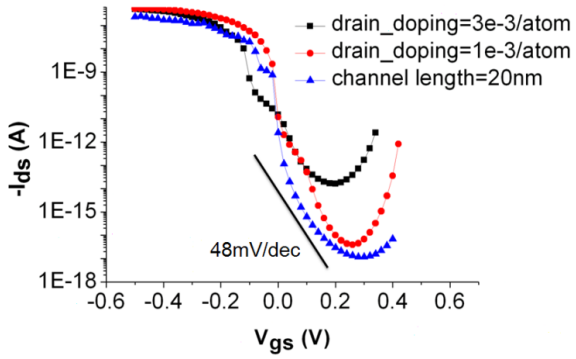

Figure 8. CNT-GNR-CNT heterojunction TFET I-V characteristics. When unzipped region (GNR) is used as a channel region, device turns on at V_{gs} <0, effectively working as a PMOS device. However, due to smaller bandgap of GNR in the channel region, weak ambipolarity is witnessed.

sufficient to have the unzipping of CNT at source/channel interface only for this particular device dimension and operation voltage range. When unzipped region (GNR) is used as a channel material (Fig. 1(b),(d)), device turns ON at V_{gs} <0 and OFF at V_{gs} >0, which effectively works as PMOS device. However, due to smaller bandgap of GNR (n=16) in the channel region, weak ambipolarity is witnessed (Fig. 8).

Subthreshold characteristics of GNR/CNT heterojunction TFET also depend on the channel length, doping and V_{ds} (Fig. 9). Direct tunneling between the source and drain dramatically increases with shorter channel length (< 15nm). Furthermore, large V_{ds} increases the device off-state tunneling through the channel-drain junction. This tunneling disappears when V_{ds} ≤0.4V and removes the ambipolarity (Fig. 9).

I_{on} of GNR/CNT heterojunction TFETs strongly depends on the injecting states from the source region. GNR-CNT-GNR and GNR-CNT-CNT configurations show comparable I_{on} as those of GNR homojunction TFETs. On the other hand, CNT-GNR-CNT and CNT-GNR-GNR show similar I_{on} to CNT TFETs. However, this is a conservative estimation, since it can be further improved by an inherent stress developed in the junction region due to the partial unzipping of the CNT [16,17].

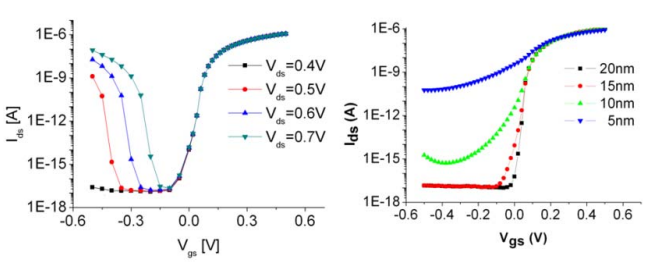

Figure 9. V_{ds} (left) and channel length (right) dependence of GNR/CNT Heterojunction TFETs. Subthreshold slope (SS) and I_{off} show dependencies on the V_{ds} (left) and the channel length (right).

Conclusion

We have investigated the performance of partially unzipped CNT heterojunctions, by means of a multi-scaled approach based on DFT, EHT, MD and self-consistent TB simulations of carrier transport. GNR/CNT heterojunctions demonstrated to be good candidates for low voltage logic applications and show better performance in terms of low subthreshold slope and strongly suppressed ambipolar behavior as compared to CNT and GNR TFETs.

Acknowledgment

G.F. and G.I. gratefully acknowledge the EC 7FP Project GRAND (Contract 215752), and the MIUR-PRIN for "Modeling and simulation of graphene nanoribbon FETs for high-performance and low-power logic applications" project (Prot. 2008S2CLJ9).

Reference

1. J. Rabaey, "Low Power Design Essentials," *Springer,* DOI 10.1007 (2009)
2. W. Choi, B. Park, J. Lee, T.K. Liu, "Tunneling Field-Effect Transistors with Subthreshold Swing (SS) less than 60mV/dec," *IEEE Electron Device Lett.*, vol. 28, no. 8, pp.743-745 (2007)
3. L. Jiao, L. Zhang, X. Wang, G. Diankov and H. Dai, "Narrow Graphene Nanoribbons from Carbon Nanotubes," *Nature*, vol. 458, pp877-880 (2009)
4. D. Kosynkin, *et al.*, "Longitudinal Unzipping of Carbon Nanotubes to form Graphene Nanoribbons," *Nature*, vol. 458, pp. 872-877 (2009)
5. K. Kim, A. Sussman, and A. Zettl, "Graphene Nanoribbons Obtained by Electrically Unwrapping Carbon Nanotubes," *ACS Nano,* vol.4, no.3 (2010)
6. Y. Yoon, S. Salahuddin, "Barrier-free tunneling in a carbon heterojunction transistor," *Appl. Phys. Lett.,* vol. 97, 033102 (2010)
7. P. Zhao, J. Chauhan and J. Guo, "Computational Study of Tunneling Transistor Based on Graphene Nanoribbon,", *Nano Lett.,* vol.9, no. 2, pp.684-688 (2009)
8. D. Kim, *et al*., "Low Power Circuit Design based on Heterojunction Tunneling Transistors (HETTs)," *Proc. Intl. Symp. Low Power Electronics and Design*, pp.219-224 (2009)
9. D. Kienle, J.I. Cerda and A.W. Ghosh, "Extended Hückel theory for band structure, chemistry, and transport. I. Carbon nanotubes," *J. Appl. Phys*, vol. 100, 043714 (2006)
10. M. Brandbyge, J.-L. Mozos, P. Ordejón, J. Taylor, and K. Stokbro, *Phys. Rev. B* vol. 65, 165401 (2002)
11. G. Fiori, G. Iannaccone, "NanoTCAD ViDES," DOI: 10254/nanohub-r5116.5, (2008)
12. S. Plimpton, "Fast Parallel Algorithms for Short-Range Molecular Dynamics," *J Comp Phys,* vol. 117, pp.1-19 (1995)
13. ITRS http://public.itrs.net
14. B. Shan, K. Cho, "First Principles Study of Work Functions of Single Wall Carbon Nanotubes," *Phys. Rev. Lett.* vol. 94, 236602 (2005)
15. Q. Yan, *et. al.,* "Intrinsic Current-Voltage Characteristics of Graphene Nanoribbon Transistors and Effect of Edge Doping," *Nano Lett.,* vol.7, no.6 pp.1469-1473 (2007)
16. J. Zhang, K. Ong and P. Wu, "The Influence of Out-of-Plane Deformation on the Bandgap of Graphene Nanoribbon," *J. Phys. Chem. C,* vol. 114, pp.12749-12753 (2010)
17. Y. Li, X. Jiang, Z. Liu and Z. Liu, "Strain Effects in Graphene and Graphene Nanoribbons: The Underlying Mechanism," *Nano Res.,* vol. 3, no. 8, pp. 545-556 (2010)